LAPP-TH-30
Ref.Th.3029-CERN
February 17, 1981

Heavy Quark jets as technicolour signatures in pp and $p\bar{p}$ collisions

G. Girardi,
LAPP, Annecy-le-Vieux, France

F. Méry*)
Theory Division, CERN

and

P. Sorba**)
LAPP, Annecy-le-Vieux, France

A B S T R A C T

Within the framework of technicolour models many heavy bosons are expected. In this paper we propose heavy quark jets as a good way to find some of these particles. Our calculation suggest that the collider at BNL is the most adequate machine for such hunting.

---

*) On leave of absence from the Centre de Physique Théorique and the Faculté des Sciences de Luminy, Marseille, France.

**) On leave of absence from the Centre de Physique Théorique, Marseille, France.

I. Introduction

An elegant way to circumvent certain difficulties presented by the Higgs mechanism for breaking gauge symmetries has been proposed and developed during the last two years[1]. The introduction of a new gauge group, called technicolour, similar to the colour strong interaction gauge group $SU(3)_c$, but with a mass scale of order 1 TeV, allows one to give the expected masses to the $W^{\pm}$ and Z gauge bosons. In such theories, the traditional Higgses are replaced by "condensates" of technicoloured fermion-antifermion (Technifermions) pairs $F\bar{F}$ acquiring a non zero vacuum expectation value. In the specific models we will refer to, the chiral flavour symmetry group for technifermions $SU(8)_L \times SU(8)_R$ is reduced to SU(8) by dynamical symmetry breaking giving rise to 63 "pseudo"-Goldstone bosons. Three of them are eaten by the $W^{\pm}$ and Z^0. The remaining ones acquire masses with the help of the $SU(3) \times SU(2) \times U(1)$ and other interactions. These "pseudo" bosons can be separated into four colour singlets, four colour triplets and antitriplets, and four colour octets. While the masses of the colour singlets are expected to be of the order of a few GeV, the masses of colour octets are supposed to be in the range 150-300 GeV. There exists at present no fully satisfactory technicolour model and various versions of this approach can have very different technifermion structures, however a common feature of all of them is the appearance of many Goldstone bosons in an accessible mass range[2]. So the observation of such particles, though it would not prove or disprove any specific model, would nevertheless give support to dynamical symmetry breaking ideas.

General calculations for the production of pseudo Goldstone bosons have already been presented[3),4),5)]. In this paper we concentrate on the possible detection of neutral colour octets $P_8^{0,3}$ (hereafter P_8) in $p\bar{p}$ and pp collisions, through their decays into high mass quark antiquark (e.g. $t\bar{t}$ pairs).

In section II we look at the general properties of these P_8 octets using their couplings to fermions coming from the assumption of "monophagy"[6], i.e. fermions with the same charge acquire their masses from the same technifermion condensate, which preserves the G.I.M. mechanism.

In section III we concentrate on the particular channel $\overset{(-)}{p}\overset{(-)}{p} \to P_8 \to t\bar{t}$ and compare it to the expected QCD background. We study the invariant mass spectrum of the $t\bar{t}$ pairs produced via the two competing mechanisms and show that a rather clear signal for the P_8 should emerge out of the continuum. Another signature for P_8 production would be the angular distribution of the jets which we have calculated. In the invariant mass spectrum, the P_8 should appear as a very narrow peak (current estimates give it a total width of a few hundred MeV), so narrow that it can be smoothed out by the mass resolution of the experiments.

In that spirit we provide histograms for the spectrum with bins in invariant mass; it appears that with a resolution of 2% in mass there is still a signal and especially for $\sqrt{s}$ = 800 GeV (cf. the Isabelle collider at BNL) the signature is clear.

II. P_8 production

The P_8 can be produced in hadronic collisions by a Drell Yan type mechanism

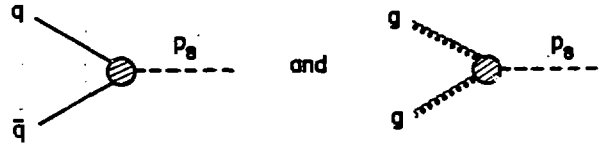

(1) (2)

Process (1) which involves a $q\bar{q}$ annihilation can be neglected with respect to the gluon "fusion" process (2). Indeed the P_8, like the other Goldstone bosons, couples to the fermions like a Higgs, that is, the heavier the fermion the stronger the coupling. In this way P_8 will preferentially couple to $t\bar{t}$ pairs, t being our nickname for the heaviest quark, which are very suppressed in the usual hadron sea, making process (1) unlikely.

The production cross-section for the $P_{8,c}$ of a definite colour index c and mass m_p is given by the following formula

$$\sigma(pp \text{ or } p\bar{p} \to gg \to P_8) = \frac{4\pi^2}{m_p^3} \sum_{a,b} \Gamma(P_{8,c} \to g_a g_b) \mathcal{L}_{ab}(\tau) . \qquad (II.1)$$

where $\mathcal{L}_{ab}(\tau)$ is the integrated luminosity of the subprocess with 2 gluons of colour index a and b

$$\mathcal{L}_{ab}(\tau) = \int_\tau^1 dx \left[g_a(x) g_b(\tau/x) + g_b(x) g_a(\tau/x) \right] \frac{\tau}{x} dx , \qquad (II.2)$$

where $\tau = \frac{m_p^2}{s}$, $\sqrt{s}$ is the total hadronic energy and x(resp $\frac{\tau}{x}$) the amount of the p(resp $\bar{p}$) momentum carried by the gluons.

Colour is summed in the proton, therefore

$$g_a(x) = g_b(x) = \frac{1}{8} G^p(x) . \qquad (II.3)$$

For the gluon distribution we have chosen a scaling parametrization $G^p(x) = 3(1-x)^5/x$, with a normalization factor to insure that gluons carry effectively half of the proton momentum. Scaling violations would modify both the P_8 production cross-section and the QCD background by the same factor. However as

we are concerned to estimate the ratio of signal to background which is insensitive to these effects the P_8 signatures will be unaffected.

Therefore, we can write

$$\mathcal{L}_{ab}(\tau) = \frac{1}{32}\int_\tau^1 G^p(x)G^p(\tau/x)\,\frac{\tau}{x}\,dx = \frac{1}{32}\,\mathcal{L}(\tau), \qquad (II.4)$$

which gives

$$\sigma(\overset{(-)}{p}\overset{(-)}{p} \to P_{8,c}) = \frac{\pi^2}{8m_p^3}\,\mathcal{L}(\tau)\;\Gamma(P_{8,c} \to gg), \qquad (II.5)$$

where $\Gamma(P_{8,c} \to gg) = \sum_{a,b}\Gamma(P_{8,c} \to g_a g_b)$.

If we sum over all the colours which can be produced we obtain

$$\sigma(\overset{(-)}{p}\overset{(-)}{p} \to P_8) = \frac{\pi^2}{m_p^3}\,\mathcal{L}(\tau)\Gamma(P_{8,c} \to gg). \qquad (II.6)$$

The decay rates for the P_8 have already been calculated[3),4),5)]. While the gluon-gluon channel can be estimated in a general model, the couplings to fermions are much more dependent on the specific model of extended technicolour (ETC) one chooses. Here we shall only consider one example given in Ref. 6) called the "first monophagic model". In this model the ETC interaction connects usual quarks to techniquarks of the same charge, for instance u,c,t quarks acquire masses from the techniquark condensate $U\bar{U}$ where U is the techniquark of charge $\frac{2}{3}$. Decay rates are then:

$$\Gamma(P_{8,c} \to 2\ gluons) = \frac{5}{3}\left(\frac{G_F}{\sqrt{2}}\right)\frac{m_p^3}{\pi}\left(\frac{\alpha_s}{\pi}\right)^2\left(\frac{N_{TC}^2}{4}\right), \qquad (II.7)$$

$$\Gamma(P_{8,c} \to q\bar{q}) = \left(\frac{G_F}{\sqrt{2}}\right)\frac{m_p}{\pi}\;m_q^2, \qquad (II.8)$$

N_{TC} being the dimension of the technicolour group.

This gives us for (II.6)

$$\sigma(\overset{(-)}{p}\overset{(-)}{p} \to ggX \to P_8 X) = \frac{5\pi}{3}\left(\frac{G_F}{\sqrt{2}}\right)\left(\frac{\alpha_s}{\pi}\right)^2\left(\frac{N_{TC}}{4}\right)^2\mathcal{L}_{gg}\left(\tau = \frac{m_p^2}{s}\right). \qquad (II.9)$$

The differential cross-section at zero rapidity can be obtained very easily

$$\left.\frac{d\sigma(\overset{(-)}{p}\overset{(-)}{p} \to P_8 X)}{dy}\right|_{y=0} = 15\pi\left(\frac{G_F}{\sqrt{2}}\right)\left(\frac{\alpha_s}{\pi}\right)^2\left(\frac{N_{TC}}{4}\right)^2\left(1 - \sqrt{\frac{m_p^2}{s}}\right)^{10}, \qquad (II.10)$$

with $y = \ln\frac{x}{\sqrt{\tau}}$.

Numerical estimates for these 2 quantities are presented in table I where we have chosen the number of technifermions per generation to be $N_{TC} = 4$. These results agree with previously quoted values[4].

Given the smallness of the calculated cross-sections it is crucial to propose clear signatures of the final states into which the P_8 can decay. A priori, the most relevant channels will be those with 2 gluons or with a pair of heavy quark-antiquark. The branching ratios given in table II estimated using (II.7) and (II.8) confirm this statement.

III. $t\bar{t}$ jets: P_8 versus QCD continuum

In this section we compare the production of heavy quark jets by the P_8 and by the QCD continuum. As emphasized in the previous section the main source of P_8 is gluon-gluon "fusion". For the QCD contribution we consider also the gluon-gluon subprocess which is the most important at high energy. For pp collisions ($\sqrt{s} = 800$ GeV) the situation is clear, but this is not so for a $p\bar{p}$ collider at a relatively lower energy like the CERN $p\bar{p}$ machine working at $\sqrt{s} = 540$ GeV. Here the $q\bar{q}$ annihilation can be competitive, but current estimates show that this process is at most of the same order as gluon-gluon collisions. So we think that using only the gluon-gluon fusion is not an unreasonable assumption.

We compute the production cross-section of a $t\bar{t}$ pair coming from P_8 in pp or $p\bar{p}$ collision, using the Drell Yan mechanism:

$$\left(\frac{d\sigma}{d\hat{s}}\right)_{P_8} = \frac{1}{s}\int_\tau^1 \frac{dx}{x}\, G(x)G(\tau/x)\hat{\sigma}(x,\frac{\tau}{x},\hat{s}). \qquad \text{(III.1)}$$

where $\sqrt{s}$ is the total energy of the process, $\hat{s}$ and $\hat{\sigma}$ correspond to the subprocess and $\tau = \frac{\hat{s}}{s}$.

As we have argued before, the dominant contribution to this subprocess corresponds to the diagram:

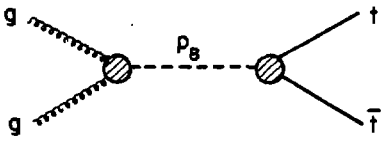

Using the property that P_8 is a pseudo scalar, we can relate the amplitudes of the two above bubbles to the partial decay rate $\Gamma(P_8 \to gg)$ and $\Gamma(P_8 \to t\bar{t})$. Therefore we get for the subprocess:

$$\hat{\sigma}(gg \to P_s \to t\bar{t}) = \frac{\pi}{2}\left(\frac{m_p}{\hat{s}}\right)^2 \left[\frac{\hat{s}(\hat{s}-4m_t^2)}{m_p^2(m_p^2-4m_t^2)}\right]^{1/2} \frac{\Gamma(P_s \to gg)\Gamma(P_s \to t\bar{t})}{(\hat{s}-m_p^2)^2 + m_p^2\Gamma_{tot}^2} \quad \text{(III.2)}$$

in which we have used the Breit-Wigner form for the P_s propagator, Γ_{tot} being the total width of the P_s.

Taking into account the expressions for the decay rates given in section II, we deduce:

$$\frac{d\sigma}{d\hat{s}} = \frac{5}{3\pi}\left(\frac{G_F}{\sqrt{2}}\right)^2\left(\frac{\alpha_s}{\pi}\right)^2 \frac{m_p^2\, m_t^2}{(\hat{s}-m_p^2)^2 + m_p^2\Gamma_{tot}^2}\left(\frac{m_p^2}{\hat{s}}\right)^2\left[\frac{1-\frac{4m_t^2}{\hat{s}}}{1-\frac{4m_t^2}{m_p^2}}\right]^{1/2} \quad \text{(III.3)}$$

$$\times \left(\frac{N_{TC}}{4}\right)^2 \tau \int_\tau^1 G(x)\, G(\tau/x)\, \frac{dx}{x}\,,$$

and:

$$\left.\frac{d\sigma}{d\hat{s}dy}\right|_{y=0} = \frac{5}{3\pi}\left(\frac{G_F}{\sqrt{2}}\right)^2\left(\frac{\alpha_s}{\pi}\right)^2 \frac{m_p^2\, m_t^2}{(\hat{s}-m_p^2)^2 + m_p^2\Gamma_{tot}^2}\left(\frac{m_p^2}{\hat{s}}\right)^2\left[\frac{1-\frac{4m_t^2}{\hat{s}}}{1-\frac{4m_t^2}{m_p^2}}\right]^{1/2} \quad \text{(III.4)}$$

$$\times\ \tau\, G(\sqrt{\tau})\, G(\sqrt{\tau}).$$

The QCD background for $t\bar{t}$ production requires the calculation of several diagrams:

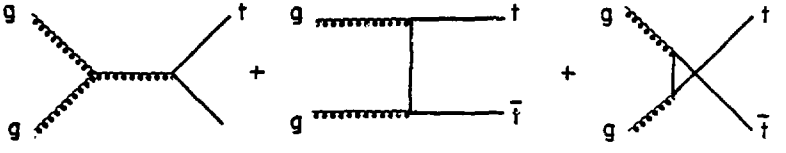

and the cross-section for this subprocess has been already calculated[7),8)].

$$\left(\frac{d\hat{\sigma}}{d\hat{t}}\right)_{QCD} = \frac{\pi\alpha_s^2}{\hat{s}^2}\left\{\frac{3(\hat{t}-m_t^2)(\hat{u}-m_t^2)}{4\hat{s}^2} - \frac{m_t^2(\hat{s}-4m_t^2)}{24(\hat{t}-m_t^2)(\hat{u}-m_t^2)} + \right. \quad \text{(III.5)}$$

$$\left[\frac{(\hat{t}-m_t^2)(\hat{u}-m_t^2) - 2m_t^2(\hat{t}+m_t^2)}{6(\hat{t}-m_t^2)} + \frac{3}{8}\frac{(\hat{t}-m_t^2)(\hat{u}-m_t^2)+m_t^2(\hat{u}-\hat{t})}{\hat{s}(\hat{t}-m_t^2)}\right]$$

$$\left. + [\hat{u} \leftrightarrow \hat{t}]\right\}.$$

where, in the c.m. of the subprocess:

$$\hat{t} = (\hat{p}_1 - \hat{p}_3)^2 = m_t^2 - \frac{\hat{s}}{2} + \sqrt{\hat{s}}\sqrt{\frac{\hat{s}}{4} - m_t^2}\cos\hat{\theta}$$
$$\text{and} \quad \hat{u} = (\hat{p}_1 - \hat{p}_4)^2 = m_t^2 - \frac{\hat{s}}{2} - \sqrt{\hat{s}}\sqrt{\frac{\hat{s}}{4} - m_t^2}\cos\hat{\theta} \qquad \text{(III.6)}$$

The kinematics being explicit on the diagram:

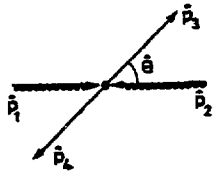

In order to compare with the $t\bar{t}$ pair production via the P_8, we have to compute:

$$\left(\frac{d\sigma}{d\hat{s}}\right)_{QCD} = \frac{1}{\hat{s}}\int_\tau^1 dx\ G(x)\ G(\tau/x)\ \frac{\tau}{x}\int_{t^-}^{t^+}\left(\frac{d\hat{\sigma}}{d\hat{t}}\right)_{QCD} d\hat{t} \qquad \text{(III.7)}$$

with $t^\pm = (m^2 - \frac{\hat{s}}{2}) \pm \frac{1}{2}\sqrt{\hat{s}(\hat{s} - 4m^2)}$ corresponding to $\cos\hat{\theta} = \pm 1$ and:

$$\left(\frac{d^2\sigma}{d\hat{s}dy}\right)_{QCD}\Big|_{y=0} = \frac{1}{\hat{s}}\tau\ G(\sqrt{\tau})\ G(\sqrt{\tau})\int_{t^-}^{t^+}\left(\frac{d\hat{\sigma}}{dyd\hat{t}}\right)_{QCD} d\hat{t}. \qquad \text{(III.8)}$$

We have plotted $\frac{d\sigma}{d\hat{s}}(\hat{s})$ for $t\bar{t}$ production from QCD (dashed line) and from P_8 (solid line) for $m_p = 150$ GeV (fig. 1) and $m_p = 300$ GeV (fig. 2). The curves are given for 3 values of the total c.m. energy: $\sqrt{s} = 540$ GeV (CERN $p\bar{p}$ collider), $\sqrt{s} = 800$ GeV (Isabelle) and $\sqrt{s} = 2000$ GeV (Fermilab TeVatron). A similar study is done in fig. 3 and 4 for $\frac{d\sigma}{d\hat{s}dy}\Big|_{y=0}(\hat{s})$.

From these curves we can notice that at values of $\sqrt{\hat{s}} = m_p$, the P_8 peak is higher by about one order of magnitude than the QCD background. The possibility to observe such an effect depends on two parameters: the P_8 mass and the total c.m. energy. The cross-section decreases as the P_8 mass increases, but increases with the total c.m. energy. From the curves, it appears that there is very little hope to observe a P_8 with the CERN $p\bar{p}$ collider ($\sqrt{s} = 540$ GeV) due to the expected luminosity. But with Isabelle or even better with the TeVatron, if the machines reach the expected luminosity, a clear signal should be observable (as an example for $\sqrt{s} = 800$ GeV, and the expected luminosity of the Isabelle machine

$L = 10^{32}\ cm^{-2}$, one would get with, $m_p = 150$ GeV and using fig. 1, a number of events at the peak equal to $5 \times 10^{-37} \times 10^{32} = 5 \times 10^{-5}$ ev/sec i.e. ~ 5 evts per 24 hours run).

Now, to see if the machine allows us to observe such a P_8 peak we have to know in which kinematical region the P_8 production is the most favoured with respect to the QCD background. We have computed the angular distribution $\frac{d\sigma}{d\hat{s}dcos\theta}$ and $\frac{d\sigma}{d\hat{s}dydcos\theta}\Big|_{y=0}$ both for P_8 production and for the QCD background, θ being the angle between the beam and the $t\bar{t}$ axis. The Drell Yan formulae for the angular distributions can be written as:

$$\frac{d\sigma}{d\hat{s}dcos\theta} = \frac{1}{s}\int_\tau^1 G(x)\ G(\tau/x)\ \frac{dx}{x}\ \frac{d\hat{\sigma}}{d\hat{s}dcos\theta}\ , \qquad \text{(III.9)}$$

and

$$\frac{d\sigma}{d\hat{s}dydcos\theta}\Big|_{y=0} = \tau\left[G(\sqrt{\tau})\right]^2 \frac{d\hat{\sigma}}{d\hat{s}dydcos\theta}\Big|_{y=0} \qquad \text{(III.10)}$$

with $\frac{d\hat{\sigma}}{dcos\theta} = \frac{d\hat{\sigma}}{dcos\hat{\theta}} \cdot \frac{dcos\hat{\theta}}{dcos\theta}$.

The quantity $\frac{dcos\hat{\theta}}{dcos\theta}$ can be calculated, as usual, using the Lorentz boost from the subprocess c.m. to the $\overset{(-)}{p}p$ c.m.

$$\frac{dcos\hat{\theta}}{dcos\theta} = \frac{4\tau}{\left[\tau/x + x + (\tau/x - x)\ cos\theta\right]^2} \qquad \text{(III.11)}$$

Due to the fact that P_8 is a pseudoscalar, the distribution $\left(\frac{d\hat{\sigma}}{dcos\hat{\theta}}\right)_{P_8}$ is isotropic, and so it will be the same for $\left(\frac{d\sigma}{d\hat{s}dydcos\theta}\right)_{P_8}\Big|_{y=0}$ because $y = 0$ implies $\frac{dcos\hat{\theta}}{dcos\theta} = 1$.

The angular distributions are plotted in fig. 5 and 6 both for the P_8 production (solid line) and for the QCD background (dashed line).

We notice that QCD is encouragingly only dominant for $cos\theta = \pm 1$. For $cos\theta = 0$, the P_8 distribution is higher by between 1 or 2 orders of magnitude.

The peak which clearly appears at the m_p mass in the above discussed curves will certainly not be directly observable experimentally. Indeed the expected width of the P_8 meson (of the order of 300 MeV in the first monophagic model) is much smaller than the energy resolution to be expected for detectors at these machines.

In order to know whether the P_8 peak will be really observable or not, we can compute histograms by integrating the differential cross-sections over intervals equal to the expected error on the energy of $t\bar{t}$ peak. In fig. 7a,b,c are plotted the integrated cross-sections

$$\int_{\hat{s}_{i-1}}^{\hat{s}_i} \frac{d\sigma}{d\hat{s}}\, d\hat{s},$$

$$\text{with:}\quad \hat{s}_i - \hat{s}_{i-1} = R\,\frac{\hat{s}_i + \hat{s}_{i-1}}{2}$$

R being the energy resolution of the machine that we have taken equal to 2%.

From fig. 7a, we see, as we have already mentioned, that there is almost no hope to observe P_8 with the CERN $p\bar{p}$ collider, first because the luminosity is much too low to observe the expected values of the cross-section, and second because the energy resolution will not be good enough to bring out the P_8 effect. However the situation looks much better with the Isabelle machine as we can see in fig. 7b. About for the TeVatron at $\sqrt{s} = 2000$ GeV, we see in fig. 7c that the effect is also clear. However, although the σ in this last case is about 7 times higher than for $\sqrt{s} = 800$ GeV, this effect could be compensated by the smaller luminosity expected in $p\bar{p}$ machines with respect to pp machines. Therefore it appears that Isabelle looks as the best machine to observe a pseudoscalar P_8. For an energy resolution R = 4% the ratio of the P_8 signal for the $t\bar{t}$ background is about 25% instead of 40% for R = 2% with $\sqrt{s} = 800$ GeV and $m_p = 150$ GeV which still make the P_8 detectable.

Conclusion

It could seem paradoxical to search for technicolour signatures through high mass coloured P_8 (between 150 and 300 GeV) rather than through colour singlets P_0 with more accessible masses (between 5 and 10 GeV). In fact in hadron-hadron collisions (pp and $p\bar{p}$) P_0 signatures will be completely hidden in the background due to the numerous resonances in the mass region and to the Drell Yan continuum[5]. This does not appear to be the case for the P_8 if their masses are as expected. As we have shown in this paper, the cross-sections at the P_8 peak are about one order of magnitude above the $t\bar{t}$ QCD background. A study of the angular distributions shows that this remains fortunately true for all values of $\cos\theta$ except for the nonobservable region $\cos\theta = \pm 1$. A simulation of the experimental situation with histograms indicates that the 800 GeV pp collider Isabelle appears to be especially suitable for tracking the P_8, compared to the $\sqrt{s} = 540$ GeV and $\sqrt{s} = 2000$ GeV $p\bar{p}$ machines.

Acknowledgements

We have enjoyed discussions with all members of the ECFA-LEP Specialized Study Group 9 on exotic particles. Special thanks are due to J. Ellis for judicious advice and encouragement.

REFERENCES

1) S. Weinberg, Phys. Rev. D13 (1976) 974; D19 (1979) 1277;
S. Dimopoulos and L. Susskind, Nucl. Phys. B155 (1979) 237;
E. Eichten and K. Lane, Phys. Letters 90B (1980) 125;
For reviews and earlier references, see:
K.D. Lane and M.E. Peskin, Moriond Lectures, Nordita preprint 80/33 (1980);
P. Sikivie, Varenna Lectures, CERN preprint TH-2951 (1980);
E. Farhi and L. Susskind, CERN preprint TH-2975 (1980).

2) S. Dimopoulos, Nucl. Phys. B168 (1980) 69;
M. E. Peskin, Nucl. Phys. B175 (1980) 197.

3) F. Hayot and O. Napoly, CEN Saclay preprint DPhT/86 (1980).

4) S. Dimopoulos, S. Raby and G.L. Kane, University of Michigan preprint UM HE 80-22 (1980).

5) G. Barbiellini et al., DESY preprint in preparation.

6) J. Ellis, M.K. Gaillard, D.V. Nanopoulos and P. Sikivie, CERN preprint TH-2938/LAPP-TH-23 (1980), to appear in Nucl. Phys. B.

7) J. Babcock, D. Sivers and S. Wolfram, Phys. Rev. D18 (1978) 162;
H. Georgi, S.L. Glashow, M.E. Machacek and D.V. Nanopoulos, Ann. of Phys. 114 (1978) 273;
K. Hagiwara and T. Yoshino, Phys. Letters 80B (1978) 282;
C.E. Carlson and R. Suaya, Phys. Letters 81B (1979) 329;
B.L. Combridge, Nucl. Phys. B151 (1979) 429.

8) C. Michael and R. Winder, Nucl. Phys. B173 (1980) 59.

Table 1

	$\sqrt{s}$ = 540 GeV		$\sqrt{s}$ = 800 GeV		$\sqrt{s}$ = 2000 GeV	
m_p(GeV)	$\frac{d\sigma}{dy}\Big\|_{y=0}$ [pb]	σ[pb]	$\frac{d\sigma}{dy}\Big\|_{y=0}$ [pb]	σ[pb]	$\frac{d\sigma}{dy}$ [pb]	σ[pb]
150	5.56	5.54	18.08	24.24	66.0	150.4
200	1.40	1.06	8.0	8.8	50.24	99.2
250	.29	0.17	3.40	3.04	37.92	65.92
300	.043	0.02	1.312	.976	28.32	44.16

Table 2

m_p(GeV)	$B(P_8 \to g\bar{g})$	$B(P_8 \to b\bar{b})$	$B(P_8 \to t\bar{t})$
150	0.08	0.03	0.86
200	0.14	0.05	0.81
250	0.2	0.05	0.71
300	0.26	0.04	0.70

FIGURE CAPTIONS

Fig. 1 The invariant mass spectrum given by the QCD continuum production of $t\bar{t}$ pairs (dashed lines) and the P_8 (m_p = 150 GeV) contribution to $t\bar{t}$ pairs (full lines), for various value of $\sqrt{s}$ corresponding to the planned machines.

Fig. 2 Same as fig. 1 for m_p = 300 GeV.

Fig. 3 The invariant mass spectrum at zero rapidity. The QCD continuum is given by dashed lines while the P_8 contribution is in full lines. $\sqrt{s}$ = 540, 800, 2000 GeV and m_p = 150 GeV.

Fig. 4 Same as fig. 3 for m_p = 300 GeV.

Fig. 5 Angular distribution ($z = \cos\theta$) of the heavy quark jets with respect to the proton beam for QCD contribution (dashed lines) and P_8 production (full lines), for $\sqrt{s}$ = 540, 800, 2000 GeV and m_p = 150 GeV.

Fig. 6 Same as fig. 5 for the angular distribution at zero rapidity.

Figs 7 a-b-c: Histograms of the invariant mass spectrum for heavy quark jets for various energies $\sqrt{s}$ = 540, 800, 2000 GeV. The dashed area shows the contribution of a P_8 of mass 150 GeV on top of the QCD continuum.

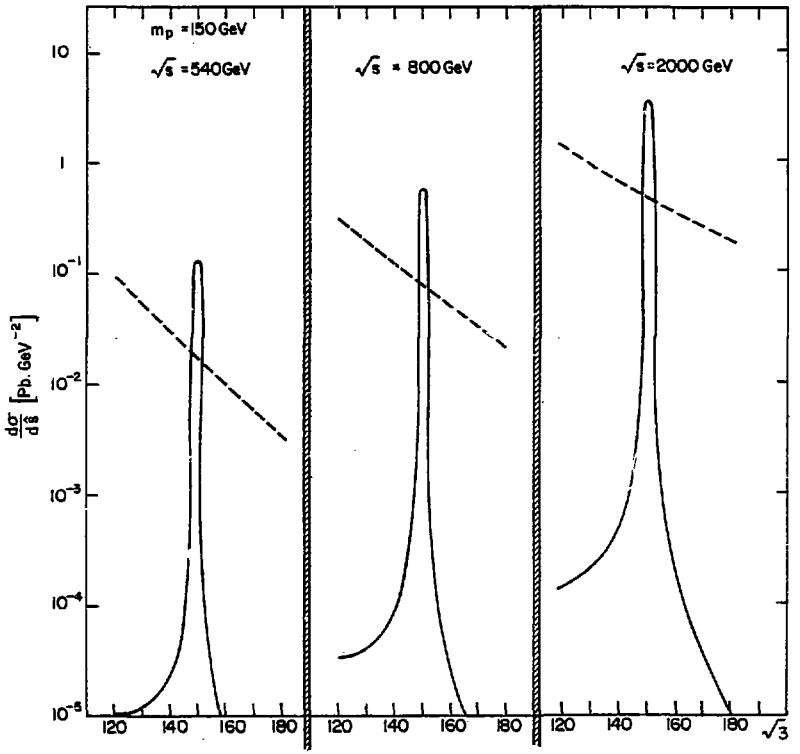
m_p = 150 GeV
$\sqrt{s}$ = 540 GeV
$\sqrt{s}$ = 800 GeV
$\sqrt{s}$ = 2000 GeV
$\frac{d\sigma}{d\hat{s}}$ [Pb. GeV^{-2}]
10
1
10^{-1}
10^{-2}
10^{-3}
10^{-4}
10^{-5}
120
140
160
180
$\sqrt{3}$

Figure 1

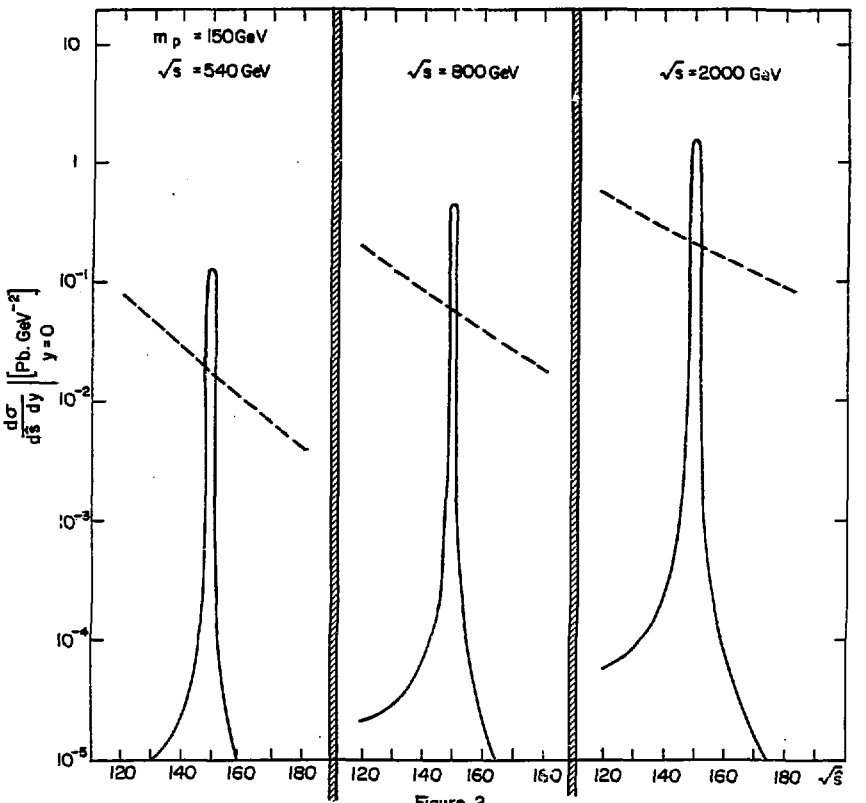
m_p = 150 GeV
$\sqrt{s}$ = 540 GeV
$\sqrt{s}$ = 800 GeV
$\sqrt{s}$ = 2000 GeV
$\frac{d\sigma}{d\hat{s}\,dy}\Big|_{y=0}$ [Pb. GeV^{-2}]
10
1
10^{-1}
10^{-2}
10^{-3}
10^{-4}
10^{-5}
120
140
160
180
$\sqrt{\hat{s}}$

Figure 2

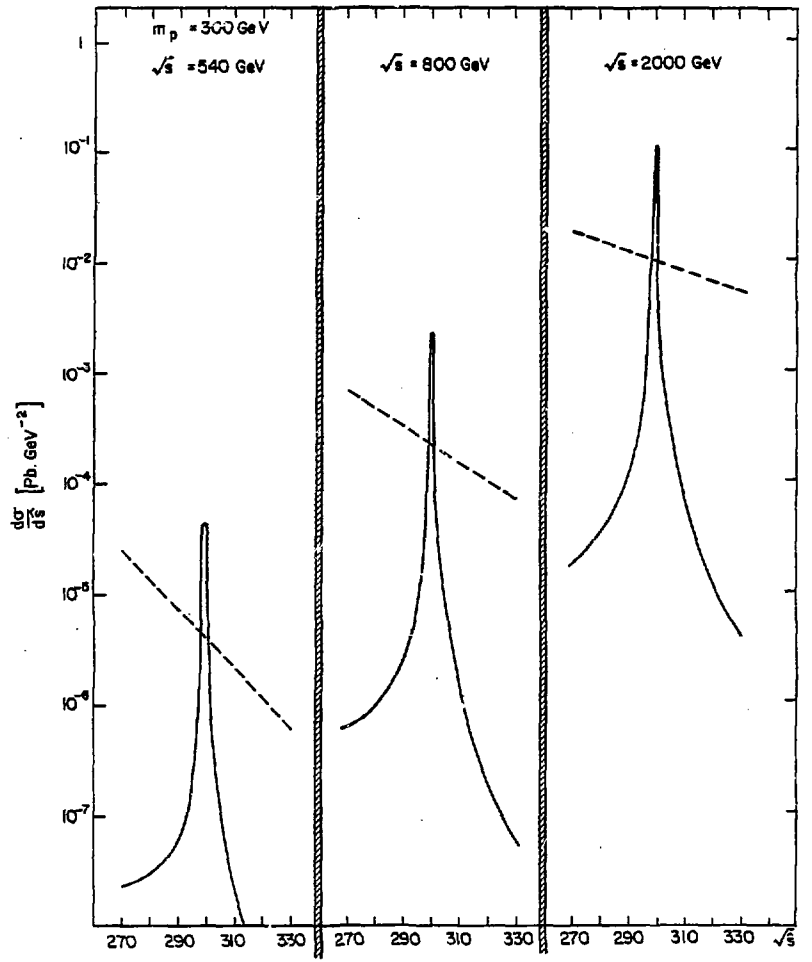
m_p = 300 GeV
$\sqrt{s}$ = 540 GeV
$\sqrt{s}$ = 800 GeV
$\sqrt{s}$ = 2000 GeV
$\frac{d\sigma}{d\sqrt{s}}$ [Pb. GeV^{-2}]
1
10^{-1}
10^{-2}
10^{-3}
10^{-4}
10^{-5}
10^{-6}
10^{-7}
270
290
310
330
$\sqrt{s}$

Figure 3

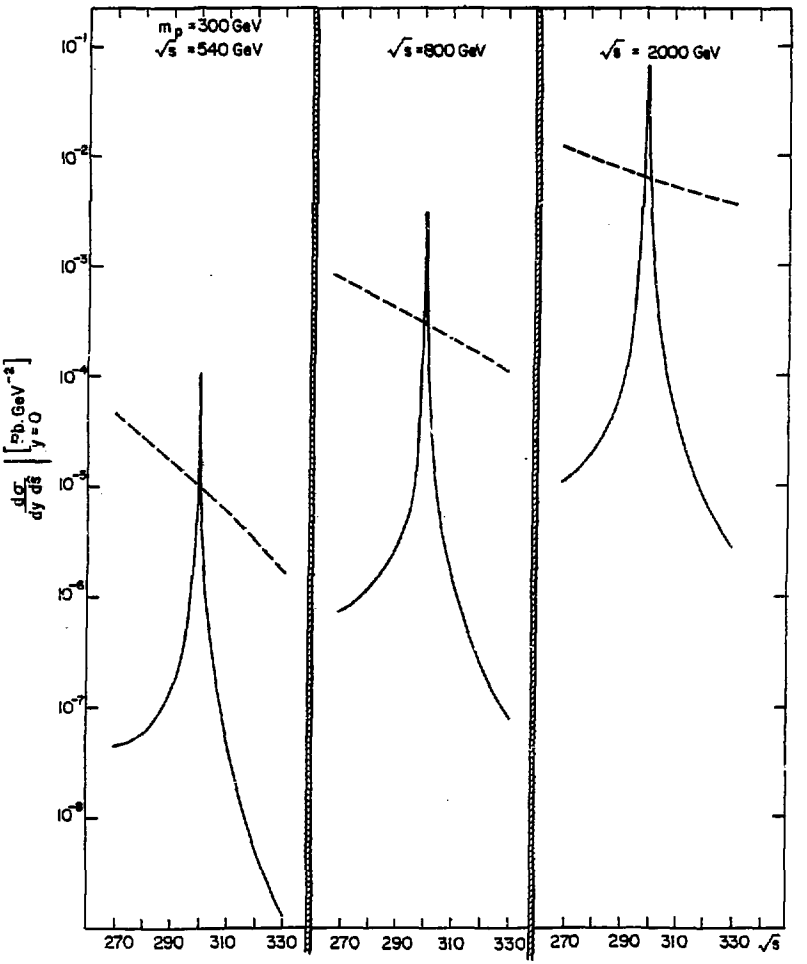
m_p = 300 GeV
$\sqrt{s}$ = 540 GeV
$\sqrt{s}$ = 800 GeV
$\sqrt{s}$ = 2000 GeV
$\frac{d\sigma}{dy\,d\hat{s}}\Big|_{y=0}$ [pb GeV^{-2}]
10^{-1}
10^{-2}
10^{-3}
10^{-4}
10^{-5}
10^{-6}
10^{-7}
10^{-8}
270 290 310 330
270 290 310 330
270 290 310 330 $\sqrt{s}$

Figure 4

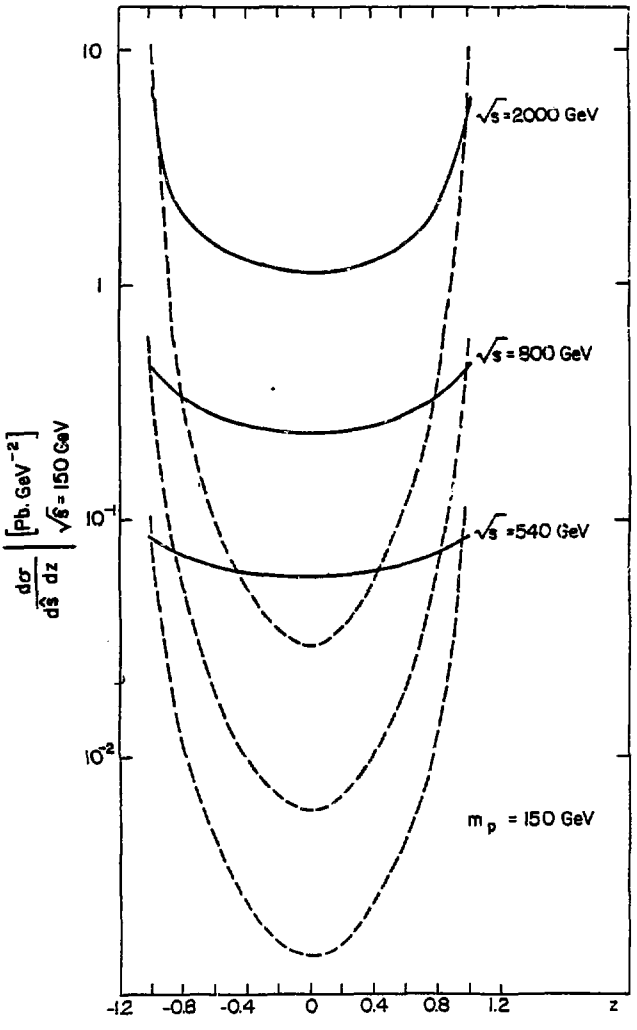
10
1
10^{-1}
10^{-2}
$\frac{d\sigma}{d\hat{s}\,dz}\Big|_{\sqrt{\hat{s}}=150\,GeV}$ [Pb. GeV^{-2}]
$\sqrt{s}$=2000 GeV
$\sqrt{s}$ = 800 GeV
$\sqrt{s}$ =540 GeV
m_p = 150 GeV
-1.2
-0.8
-0.4
0
0.4
0.8
1.2
z

Figure 5

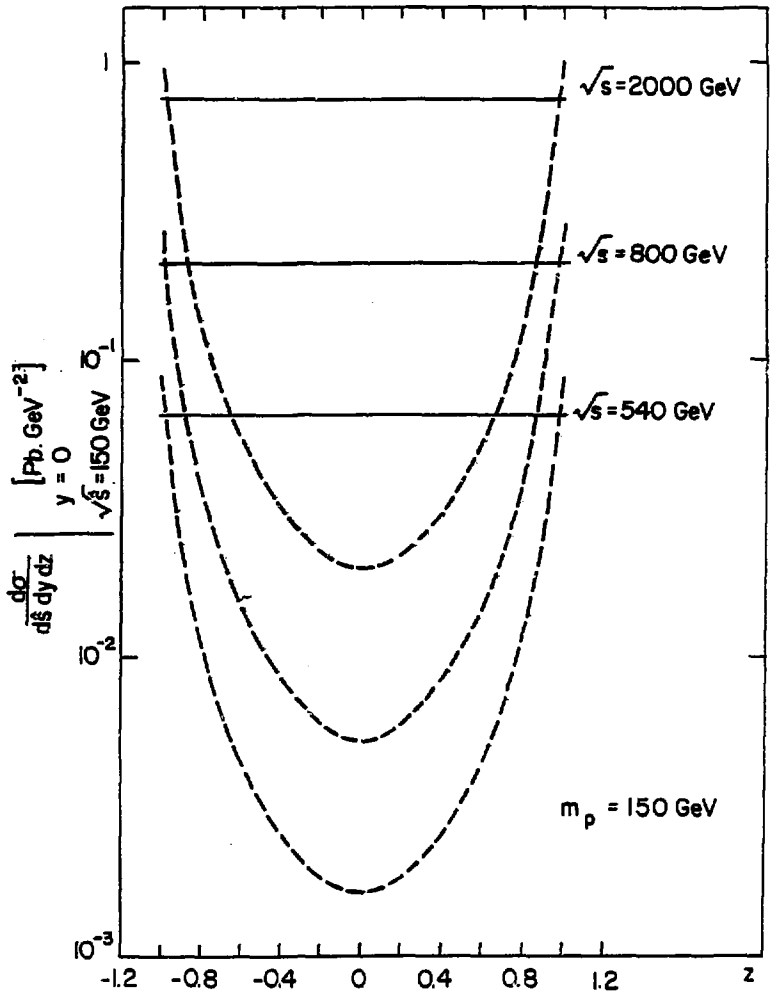
√s=2000 GeV
√s=800 GeV
√s=540 GeV
m_p = 150 GeV
dσ/dŝ dy dz [Pb. GeV^-2]
y = 0
√ŝ = 150 GeV
10^-1
10^-2
10^-3
-1.2
-0.8
-0.4
0
0.4
0.8
1.2
z

Figure 6

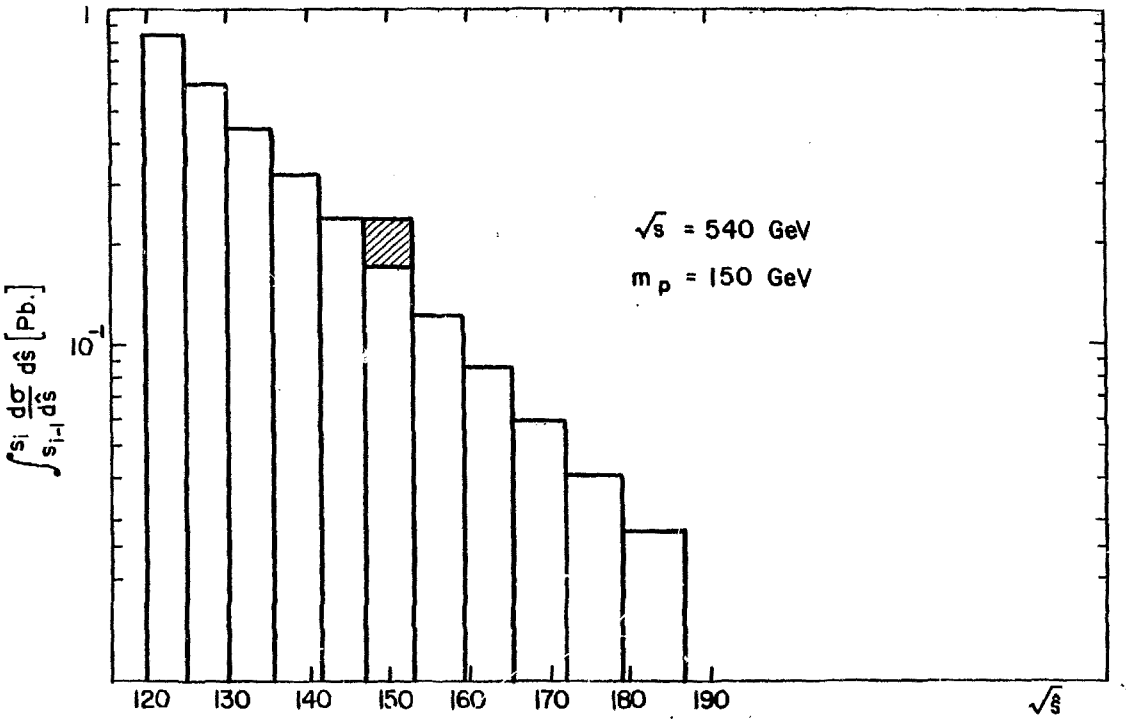
1
10^{-1}
$\int_{s_{i-1}}^{s_i} \frac{d\sigma}{d\hat{s}} d\hat{s}$ [Pb.]
$\sqrt{s}$ = 540 GeV
m_p = 150 GeV
120
130
140
150
160
170
180
190
$\sqrt{\hat{s}}$

Figure 7a

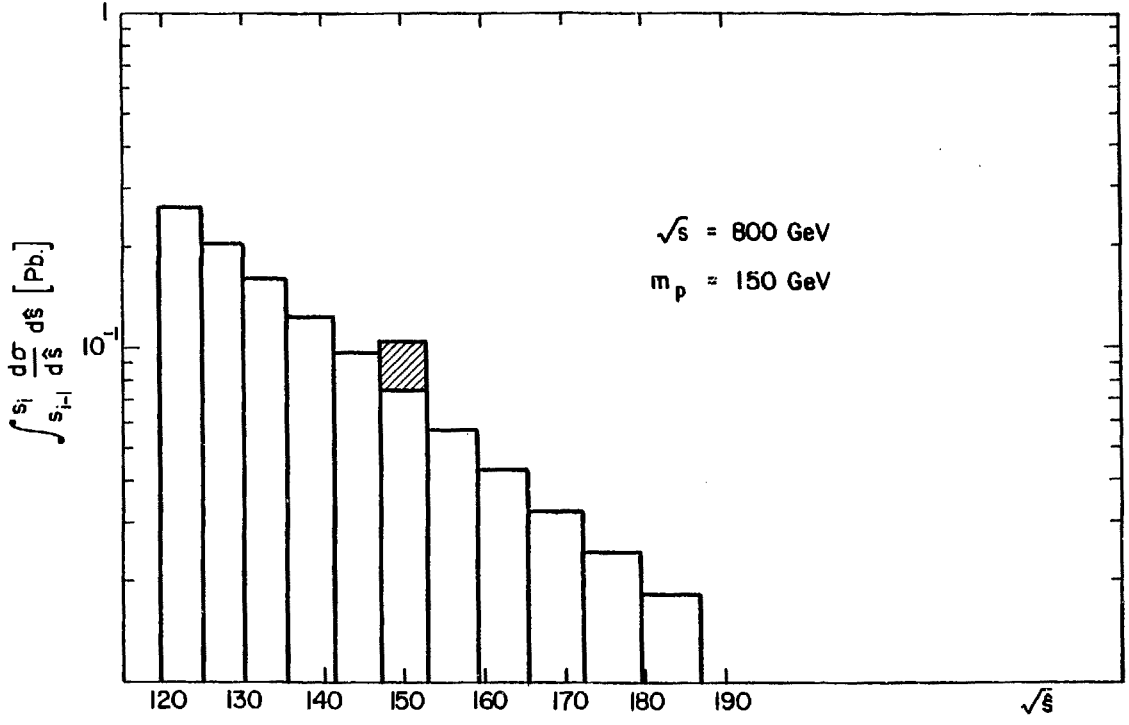
1
10^{-1}
$\int_{s_{i-1}}^{s_i} \frac{d\sigma}{d\hat{s}} d\hat{s}$ [Pb.]
$\sqrt{s}$ = 800 GeV
m_p = 150 GeV
120
130
140
150
160
170
180
190
$\sqrt{\hat{s}}$

Figure 7b

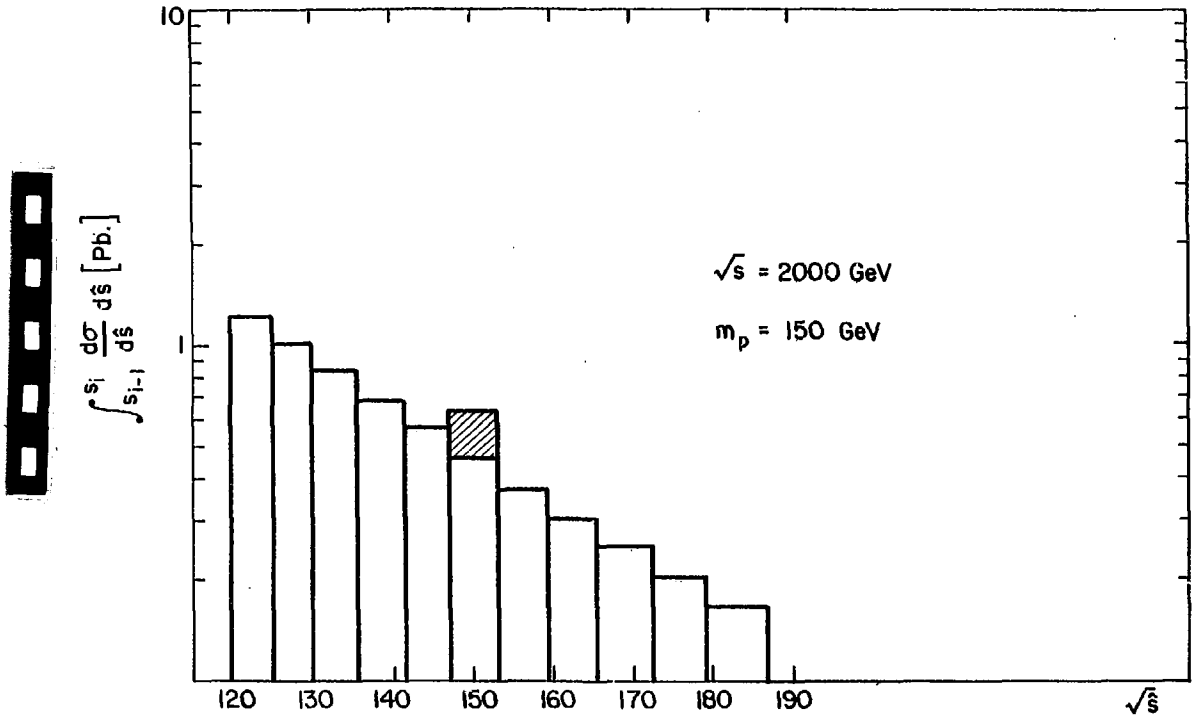
10
1
$\int_{s_{i-1}}^{s_i} \frac{d\sigma}{d\hat{s}} d\hat{s}$ [Pb.]
$\sqrt{s}$ = 2000 GeV
m_p = 150 GeV
120
130
140
150
160
170
180
190
$\sqrt{\hat{s}}$

Figure 7c